Observational Properties of Type Ib/c Supernova Progenitors in Binary Systems

Hyun-Jeong Kim[1], Sung-Chul Yoon[2], and Bon-Chul Koo[3]
Department of Physics and Astronomy, Seoul National University, Gwanak-ro 1, Gwanak-gu, Seoul 151-742, Korea

ABSTRACT

In several recent observational studies on Type Ib/c supernovae (SNe Ib/c), the inferred ejecta masses have a peak value of 2.0 – 4.0 $M_{\odot}$, in favor of the binary scenario for their progenitors rather than the Wolf-Rayet star scenario. To investigate the observational properties of relatively low-mass helium stars in binary systems as SN Ib/c progenitors, we constructed atmospheric models with the non-LTE radiative transfer code CMFGEN, using binary star evolution models. We find that these helium stars can be characterized by relatively narrow helium emission lines if the mass-loss rate during the final evolutionary phase is significantly enhanced as implied by many SN Ib/c observations. The optical brightness of helium star progenitors can be meaningfully enhanced with a strong wind for $M \gtrsim 4.4\ M_{\odot}$, but hardly affected or slightly weakened for relatively low-mass of $\sim 3.0\ M_{\odot}$, compared to the simple estimate using blackbody approximation. We further confirm the previous suggestion that the optical brightness would be generally higher for a less massive SN Ib/c progenitor. In good agreement with previous studies, our results indicate that the optical magnitudes and colors of the recently detected progenitor of the SN Ib iPTF13bvn can be well explained by a binary progenitor with a final helium star mass of about 3.0 – 4.4 $M_{\odot}$.

Subject headings: binaries: general — stars: atmospheres — stars: evolution — supernovae: general — supernovae: individual (iPTF13bvn)

1. Introduction

It is well known that the majority of massive stars are born in multiple systems, and binary systems play an important role for core-collapse supernovae (SNe). Recent observations indicate that a large fraction of massive binary stars are in relatively short-period orbits, implying that they would undergo binary interactions during the course of their evolution (Sana et al. 2012). Furthermore, the mass ratios of the stellar components of massive binary systems are found to be close to one for many cases, providing a favorable condition for stable mass transfer to avoid mergers (Kobulnicky & Fryer 2007). These findings strengthen the long-standing argument that binary interaction should be considered one of the primary factors for massive star evolution, and that binary stars may not only be related to certain exotic SNe, but also to commonly observed ones including Type Ib/c supernovae (SNe Ib/c) (e.g., Posdiadlowski et al. 1992; Woosley et al. 1995; Wellstein & Langer 1999; Eldridge et al. 2008; Yoon et al. 2010; Smith et al. 2011) .

SNe Ib/c, which constitute about 25% of all core-collapse SNe (Smith et al. 2011; Eldridge et al. 2013), are therefore important to constrain the evolution of massive stars. The hydrogen envelopes of the progenitors of these SNe must have been stripped off before they exploded. Both mass loss from single stars and binary interactions can fulfill this condition, but the resulting properties of SN Ib/c progenitors would be

[1]hjkim@astro.snu.ac.kr
[2]yoon@astro.snu.ac.kr
[3]koo@astro.snu.ac.kr

very different from each other (Yoon et al. 2012; Eldridge et al. 2013). Single Wolf-Rayet (WR) stars in the nearby Universe have bolometric luminosities of $\log L/L_{\odot} \gtrsim 5.1$, implying that their masses are higher than about 10 $M_{\odot}$. Their final masses at the pre-SN stage are predicted to be higher than about 7 $M_{\odot}$. By contrast, lower final masses are strongly preferred in binary progenitors. Recent analyses on the light curves of SNe Ib/c indicate that SN Ib/c ejecta masses are typically around 1.0–5.0 $M_{\odot}$ (Drout et al. 2011; Cano 2013; Lyman et al. 2014; Taddia et al. 2015), supporting the binary scenario over the WR star scenario.

However, the debate on which type of progenitors between single WR stars and relatively low-mass helium stars in binary systems is the dominant one for SNe Ib/c is still on-going (see Yoon 2015, for a recent review). The best way to resolve the issue would be therefore to directly identify SN Ib/c progenitors in pre-SN images (Smartt 2009). The previous searches have not been successful (Crockett et al. 2007; Smartt 2009; Eldridge et al. 2013), except for the tentative identification of the progenitor of the SN Ib iPTF13bvn (Cao et al. 2013).

Yoon et al. (2012) made rough estimates on the optical magnitudes of SN Ib/c progenitors at the pre-SN stage using their evolutionary models of massive stars. They concluded that WR progenitors would be generally very faint in the optical ($M_V \approx -2 \sim -3$ mag) compared to most WR stars observed in the nearby Universe, while relatively low-mass helium star progenitors in binary systems can be much brighter in the optical, as they become helium giant stars. Eldridge et al. (2015) also made a similar conclusion on binary progenitors. But this conclusion is based on the simple assumption of blackbody radiation from the adopted stellar evolution models. In reality, both absorption and emission lines from helium stars may have a significant impact on the optical brightness, depending on the surface temperature and the mass-loss rate by winds.

Groh et al. (2013b) and Groh et al. (2013a) presented stellar atmospheric models of single WR type progenitors at the pre-SN stage using the stellar evolution models of the Geneva group. They concluded that WO type progenitors, of which the initial masses are higher than about 35 $M_{\odot}$, would be relatively faint in the optical, in good agreement with Yoon et al. (2012), and that WN type progenitors, which are expected for a limited initial mass range ($M = 31 - 35$ $M_{\odot}$; but see Eldridge et al. 2015), can have optical magnitudes of about $-5.5 \sim -6.5$ mag. However, there exists no such a study on binary progenitors.

The purpose of this paper is therefore to present stellar atmospheric models of binary progenitors of SNe Ib/c, for the first time. This would allow to better test the binary progenitor scenario with iPTF13bvn as well as future observations. In Sect. 2, we explain our numerical methods and the adopted physical assumptions. The result of our calculations is summarized in Sect. 3. We compare our model spectra with those of HD 45166 and υ Sgr which are relatively low-mass helium stars observed in our Galaxy, as well as WN stars in Sect. 4. The predicted optical magnitudes and the implications for the progenitor of iPTF13bvn are discussed in Sects. 5 and 6. We conclude this study in Sect. 7.

2. Physical assumptions

The helium star progenitor models for the present study were chosen from the binary evolution models by Yoon et al. (2010). These models were calculated at solar metallicity including the effects of rotation, and followed up to the end of core neon burning, which is about one year before core collapse. The surface properties of these models remain almost unchanged during the final evolutionary stages after carbon exhaustion, which last for about 100 years. The pre-SN images used for the searches of SN Ib/c progenitors were usually taken about 10 years before the SN explosion (e.g., Crockett et al. 2007; Cao et al. 2013) and therefore any model after core carbon exhaustion are suitable for comparison with observations. The models chosen for atmospheric calculations are the last computed models of the sequences 5, 22 and 27, which have the final masses of 3.0, 4.4, and 5.1 $M_{\odot}$, respectively. The initial masses of these models are 14, 18, and 25 $M_{\odot}$, respectively. The optical luminosity of a helium star at the pre-SN stage is a sensitive function of its mass and radius (Yoon et al. 2012). Yoon et al. (2010) showed that there exists a fairly good mass-radius

relation for binary SN Ib/c progenitors at the pre-SN stage, and therefore these selected models can roughly represent the surface properties of SN Ib/c progenitors for the given final masses.

Given the neutron star remnant mass of about 1.3 $M_\odot$, this range of helium star masses is consistent with the peak values of the SN Ib/c ejecta mass distribution (i.e., $M_{\rm ej} \approx 2-4\ M_\odot$) inferred from SN light curves (Drout et al. 2011; Cao et al. 2013; Lyman et al. 2014). It also fits well with the inferred ejecta mass of iPTF13bvn ($M_{\rm ej} \approx 2.0\ M_\odot$; Fremling et al. 2014; Bersten et al. 2014), and thus we can directly compare our result to the observed properties of the tentative iPTF13bvn progenitor.

Yoon et al. (2010) adopted the WR mass-loss rate given by Hamann et al. (1995) using a reduction factor of 5 - 10 to consider the effect of WR wind clumping. However, the resulting wind mass-loss rates of these models are not high enough to have an optically thick WR type wind, in particular for 3.0 and 4.4 $M_\odot$ helium stars, given that their masses are relatively low and that their envelopes have relatively large radii. But the mass-loss rates from helium stars of the considered mass range are not well constrained by observations. These helium stars undergo very rapid increase in the surface luminosity as they approach to the pre-SN stage (Yoon et al. 2010, 2012), and we cannot exclude the possibility that mass loss becomes dramatically strong during this final stage (i.e., $\dot{M} \gtrsim 10^{-5}\ M_\odot\ {\rm yr}^{-1}$), which is in fact implied by many SN Ib/c observations (e.g., Foley et al. 2007; Pastorello et al. 2008; Wellons et al. 2012; Gorbikov et al. 2014). Therefore, we also consider an arbitrarily enhanced mass-loss rate for each helium star model as summarized in Table 1. Here, the label w1 denotes the models with the mass-loss rates used by Yoon et al. (2010), and w2 the models with the enhanced mass-loss rates.

The spectra of our SN Ib/c progenitor models were computed using the non-local thermodynamical equilibrium atmospheric radiative transfer code CMFGEN (Hillier & Miller 1998; Hillier 2003). CMFGEN determines the temperature distribution of the expanding atmosphere by solving the statistical and radiative equilibrium equations, and computes line and continuum formation with the spherical symmetric geometry (Hillier 1990). CMFGEN uses the super-level approach to fully treat line blanketing. In this approach, levels with similar excitation energies are grouped into a single level, under the assumption that the departure coefficients in a group are identical, and only the population of the super level is solved to to specify the populations of the levels within a super level (Hillier & Miller 1998; Hillier 2003).

CMFGEN requires a complete (previously converged) model including atmospheric structure, atomic models and their departure coefficients as the initial trial solution. For our calculations, we first adopted one of the pre-calculated O star models provided by Hillier[1] with the effective temperature of 27,500 K and Log g of 3.25, which are similar to those of our 4.4 $M_\odot$ helium star (Table 1). Table 2 presents the atomic species included in our calculations with the numbers of super and full levels. The atomic data and information on the levels are accompanied with the CMFGEN code. Once we obtained the converged model for 4.4 $M_\odot$ helium stars, we used it as the initial trial solution for the other models. The atomic models from the above O star do not include neutral and low-excitation level metal lines, which may be relevant for our 3.0 $M_\odot$ model, but this does not significantly affect the main conclusions of our study as explained in Section 4 below.

While a hydrostatic solution for the subsonic part is self-consistently solved by CMFGEN, it does not solve the momentum equation of the wind, and thus the wind velocity profile needs to be specified. For the wind part, we assume the standard β-type velocity law. We used $\beta = 1$ and 1.5 and $v_\infty/v_{\rm esc} = 2.0$ and 1.5 for the optically thin wind models (w1) and the WR-type wind models (w2), respectively (cf. Vink & de Koter 2005), where v_∞ and $v_{\rm esc}$ respectively denote the terminal wind velocity and the escape velocity. The velocity structure is modified at depth to smoothly match the structure at the surface of the hydrostatic core (for details on the CMFGEN calculations, see Hillier 1990; Hillier & Miller 1998; Hillier 2003).

Yoon et al. (2010) considered massive companion stars of OB type in their calculation. The companion star masses of the chosen progenitor models ($M = 3.0, 4.4,$ and $5.1\ M_\odot$) at the end of the calculation are 18, 23, and 35 $M_\odot$, re-

[1] http://kookaburra.phyast.pitt.edu/hillier/web/CMFGEN.htm

spectively. Note that these are not unique solutions. Yoon et al. (2010) followed the spin-up of mass accreting star as a result of mass and angular momentum accretion and the resulting enhancement of mass loss, and thus the mass transfer process is highly non-conservative in their calculations. However, the companion star masses can significantly vary according to the adopted mass accretion efficiency (i.e., the ratio of the transferred mass to the accreted mass). For example, if the mass transfer were conservative, a binary system where both stars have an initial mass of about 20 $M_{\odot}$ could produce a 3 $M_{\odot}$ helium star that has a structure similar to that of the 3.0 $M_{\odot}$ models of the present study, via Case A and AB mass transfers. The corresponding companion star mass would be about 35 $M_{\odot}$ in this case (cf. Wellstein & Langer 1999).

Given that many different combinations of helium star and companion star masses are possible in principle, we included O-type star models of three different masses (M = 20, 30, and 35 $M_{\odot}$) in the CMFGEN computation to investigate how a luminous O-type star companion would influence the optical brightness of SN Ib/c progenitor systems. These masses were chosen mainly because they can give the best fit with the observational properties of the iPTF13bvn progenitor candidate as discussed below. The 20 and 30 $M_{\odot}$ models are non-rotating models without overshooting in their early stages of the main sequence that are close to the zero-age main sequence. The 35 $M_{\odot}$ model is the last computed companion star model of the sequence 27 of Yoon et al. (2010) (i.e, the sequence for the 5.1 $M_{\odot}$ helium star model in the present study).

The model parameters are summarized in Table 1. The table lists two kinds of temperature and radius. The values of $T_{\star}$ and $R_{\star}$ are predicted from the stellar evolution code (Yoon et al. 2010) without correcting the optical depth effects from the wind, whereas the effective temperature ($T_{\rm eff}$) and photospheric radius ($R_{\rm phot}$) are the outputs from the CMFGEN calculations defined at the layer where the Rosseland optical depth ($\tau_{\rm ross}$) is 2/3. In the calculations, hydrodynamic clumping in the wind is considered by adopting a volume filling factor (f). For all models, we assume $f = 0.1$. The surface abundances were taken from the data of the selected evolutionary models.

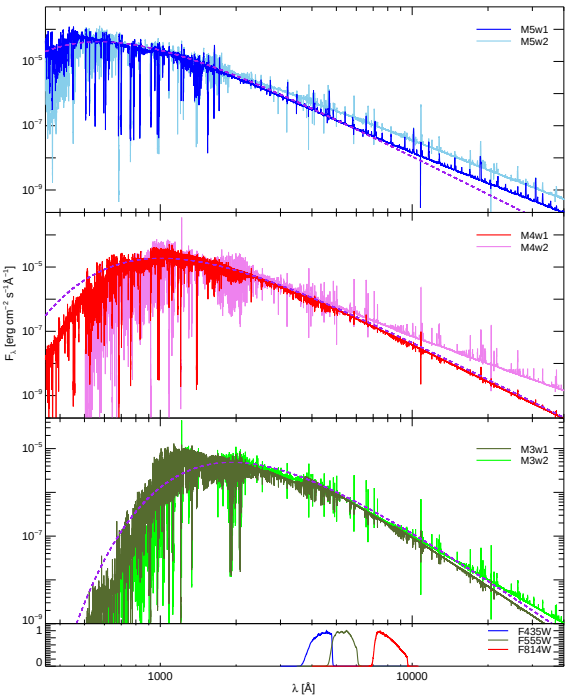

Fig. 1.— SEDs of the helium star models and the blackbody fluxes (purple dashed line) of the given temperature $T_{\star}$ and luminosity of each mass model. All fluxes are scaled to a distance of 10 pc. Transmission curves of the *HST*/ACS Wide Field Channel filters, *F435W*, *F555W*, and *F814W* are also presented at the bottom panel.

3. Results of the atmospheric models

Spectral energy distributions (SEDs) of the helium stars from the CMFGEN calculations are shown in Figure 1. All fluxes are scaled to a distance of 10 pc. The SEDs of the w1 and w2 cases for a given helium star mass are almost similar to each other, but the w2 models have excess in long wavelengths because of the extended photosphere radius with an optically thick wind. For comparison, we also present the blackbody fluxes of the given temperature ($T_{\star}$) and luminosity for each model. In optical wavelength ranges, the differences between the blackbody fluxes and the helium star models are not significant. However, the w2 models, particularly for M = 4.4 and 5.1 $M_{\odot}$, show strong excess in continuum as well as a wealth of emission lines in the optical. The large differences in the extreme ultraviolet wave-

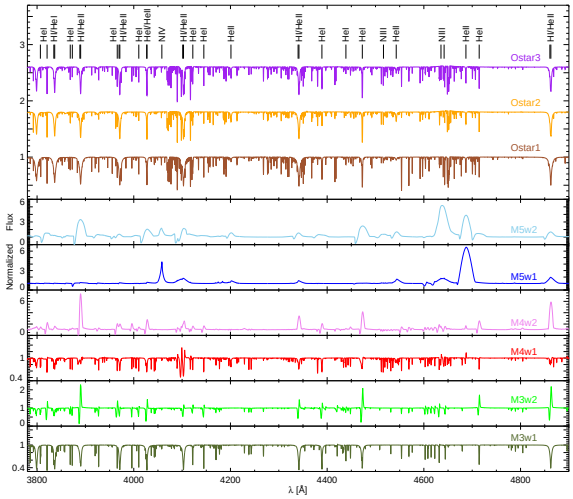

Fig. 2.— Normalized optical spectra of the helium star and O-type star models for the wavelength range of 3750 Å $\leq \lambda \leq$ 4900 Å.

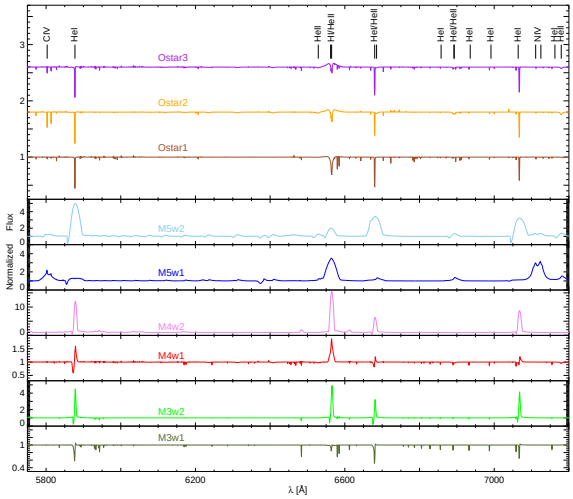

Fig. 3.— Normalized optical spectra of the helium star and O-type star models for the wavelength range of 5750 Å $\leq \lambda \leq$ 7200 Å.

lengths are owing to the line blanketing effect.

Figures 2 and 3 present the normalized optical spectra of all models. While the spectra of O-type stars only show absorption lines, those of helium stars (particularly the w2 models) show emission lines in general. The 3.0 $M_\odot$ models and the 4.4 $M_\odot$ model with w1 type wind (M3w1, M3w2, and M4w1) dominantly show absorption lines; however, compared to O-type stars, He I lines of the helium stars are broader with developed wings (e.g., He I λ4024 or He I λ4472), and they sometimes appear as (weak) P Cygni profiles (e.g., He I λ6679 or He I λ7067). In addition, the Hα line of the M4w1 model appears in emission[2]. These emission lines make the helium star to be distinguishable from O stars with a similar temperature and mass-loss rate. The H lines in the M3w1 model are absorption lines and weaker than those of O-type stars because of the lower abundance of hydrogen (see Table 1). The spectra of the 5.1 $M_\odot$ models of which hydrogen is almost depleted show broad helium emission lines and high-ionization lines such as N III/IV.

4. Comparison with Observational Counterparts

One of the observational counterparts of binary SN Ib/c progenitors is the quasi-WR (qWR) star HD 45166, which is composed of a helium rich 4.2 $M_\odot$ star with $R \simeq 1.0\ R_\odot$ and a 4.8 $M_\odot$ main sequence star (B7V) in a 1.596 day orbit (Willis & Stickland 1983; Steiner & Oliveira 2005; Groh et al. 2008). The optical spectrum of the helium star that is likely on the helium main sequence shows a number of emission lines such as He I/II, N III/IV/V, and C III/IV, and it is well explained by a model with $T_{\rm eff} = 50,000 \pm 2,000$ K ($T_\star = 70,000 \pm 20,000$ K), $\log(L/L_\odot) = 3.75 \pm 0.08$, and $\dot{M} = 2.2 \times 10^{-7}\ M_\odot\ {\rm yr}^{-1}$ (Groh et al. 2008). The spectrum of the qWR star in HD 45166 with weak He I lines and higher-ionization lines (e.g., N IV or C IV) is different from our helium star model spectra of similar mass (M4w1 and M4w2), which dominantly show He I lines. This difference is likely due to the much lower effective temperature ($T_{\rm eff}$ = 20,000–30,000 K) of our 4.4 $M_\odot$ models. As discussed in Yoon et al. (2010, 2012), low-mass (M = 3–5 $M_\odot$) helium stars are hot and visually very faint on the helium main sequence but

[2] As discussed by Yoon et al. (2010) in detail, the surface mass fraction of hydrogen for the 3.0 and 4.4 $M_\odot$ models is about 0.01 (Table 1). Hydrogen lines are actually detected in many SNe classified as Type Ib (e.g., Deng et al. 2000; Branch et al. 2002; Elmhamdi et al. 2006; Spencer & Baron 2010), and this theoretical prediction of the tiny amounts of hydrogen in some SN Ib/c progenitors is consistent with observations (see also Dessart et al. 2011).

become cooler and more luminous during the final evolutionary stages because of the rapidly expanding envelopes. The qWR star in HD 45166 is in fact much fainter in the optical ($M_V = -0.21$ mag; Willis & Stickland 1983) than our 4.4 $M_\odot$ models ($M_V \approx -5$ mag, see Section 3).

Another observational counterparts are evolved helium giant stars in binary systems. Only four stars of such a system are currently known including υ Sgr, KS Per, LSS 1922, and LSS 4300 (Dudley & Jeffery 1993), and the υ Sgr system among them has been best studied. The primary star of the υ Sgr system is a hydrogen-deficient star with $M \sim 3.0\ M_\odot$, $T_{\rm eff} \sim 12,000$ K, and $\log L/L_\odot \simeq 4.6$ (Saio 1995; Kipper & Klochkova 2012), which are comparable to those of our 3.0 $M_\odot$ helium star models. The main characteristics of the υ Sgr spectrum includes He I absorption lines, a large number of absorption/emission lines of neutral and ionized metals from low excitation levels, some P Cygni profiles, and the forbidden lines of low-ionization metal lines (Figure 4; Kipper & Klochkova 2012). He I absorption lines and metallic lines such as C II, N II, or Fe III present similar characteristics for the υ Sgr spectrum and the M3w1 model spectrum. Bonneau et al. (2011) argue that the hydrogen P Cygni profiles of the υ Sgr originate either from the circumbinary disk of this system or from the disk around the unseen secondary star. This implies that the wind mass-loss rate from the υ Sgr is comparable to the value adopted for M3w1 model that do not show emission lines, rather than that of M3w2 model for which the spectrum is characterized by strong emission lines for both hydrogen and helium (Figures 2 and 3). A number of other absorption lines only seen in the υ Sgr spectrum are neutral and metal lines of low excitation levels (e.g., N I, Ne I, or Fe II), which are not included in our models.

Finally, the spectrum of the M5w2 model may be compared with the spectra of WN stars with similar temperatures. In the M5w2 model spectrum (Figures 2 and 3), helium and nitrogen lines are dominantly observed, and most helium lines are broad and appear as P Cygni profiles. These spectral characteristics can also be found in the spectra of WN stars (Hamann et al. 2006). In particular, WN8 stars with $T_\star \simeq$ 40,000-50,000 K show very similar spectra with strong He I lines

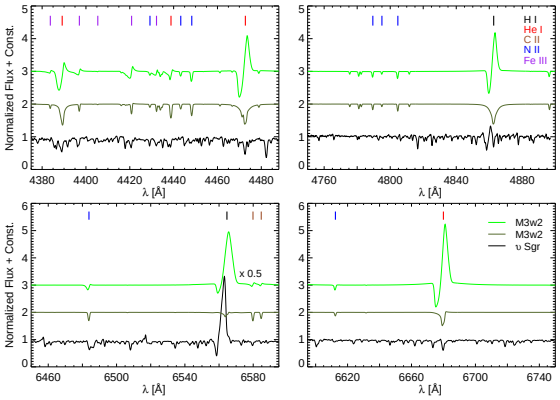

Fig. 4.— Comparison of the υ Sgr spectrum (black) that was obtained by a 60-centimetre telescope at the Observatoire du Pic du Midi on July 24, 2008, which is available from the BeSS database (http://basebe.obspm.fr/basebe), with the 3.0 $M_\odot$ helium star model spectra (dark green and light green for M3w1 and M3w2, respectively). Vertical lines at the top of each panel mark spectral lines seen in the both υ Sgr and helium star models. Black, red, brown, blue, and purple lines correspond to H I, He I, C II, N II, and Fe III, respectively. In the lower left panel, the M3w2 spectrum is scaled to 50% for display.

and negligibly weak C IV line (at 5803Å) as seen in the M5w2 model spectrum. As moving toward earlier type WN stars (i.e., higher surface temperature), He I lines become weaker and the C IV λ5803 line becomes stronger. Compared to WN8 star spectra (e.g., WR012, WR040, or WR170 in Hamann et al. 2006), however, in the M5w2 model spectrum He I lines tend to be stronger, and the N III λ4635/41 line is stronger than the He II λ4687 line. In addition, in spite of similar temperature, the M5w2 model is fainter in the optical ($M_V \gtrsim -5$ mag, see Section 3) than WN8 stars ($M_V \sim -7$ mag; Hamann et al. 2006), which is a natural consequence of the lower bolometric luminosity for the given surface temperature. Compared to the case of M5w2, in the spectrum of M5w1 the lines from higher excitation species such as N IV or C IV are stronger and He I lines almost disappear likely due to higher effective temperature compared to the M5w2 model (Table 1).

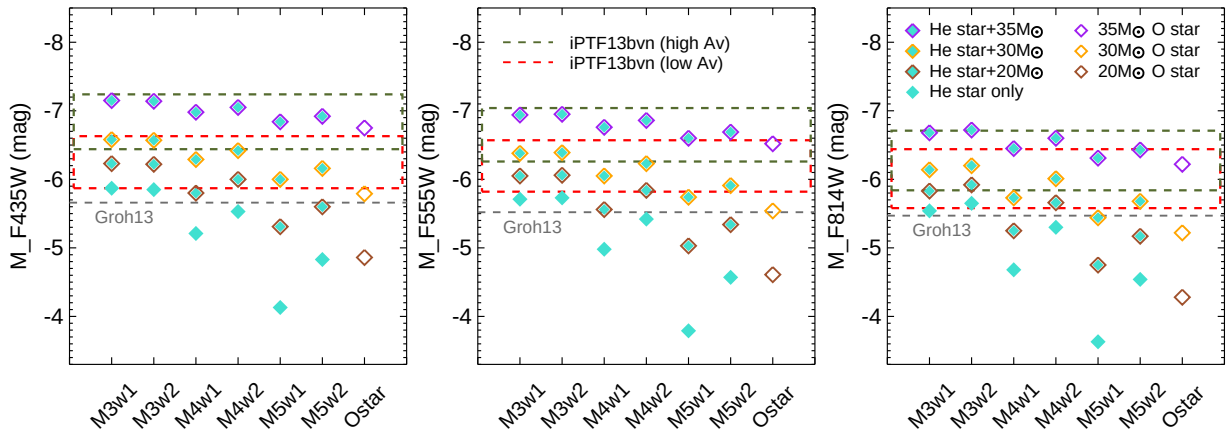

Fig. 5.— Predicted absolute magnitudes of the models in the *HST*/ACS *F435W (left)*, *F555W (middle)*, and *F814W (right)* filters. Filled cyan diamonds without borders are the absolute magnitudes of the helium star models for given *HST*/ACS filters, and open diamonds of brown, yellow, and purple are the magnitudes of 20, 30, and 35 $M_{\odot}$ O-type stars, respectively. The filled cyan diamonds with borders are the predictions of the helium stars in binary systems with an O-type star companion of corresponding colors. The extinction-corrected magnitude ranges of the iPTF13bvn progenitor candidate by the low ($E(B-V) = 0.0715$, Cao et al. 2013) and high ($E(B-V) = 0.2147$, Bersten et al. 2014) extinction values are presented with red and dark green dashed boxes, respectively. Gray dashed lines present the prediction of 32 $M_{\odot}$ WR star progenitor model from Groh et al. (2013a).

5. Absolute Magnitudes of Helium Star Binary Progenitors

In Table 3 and Figure 5, we present the predicted magnitudes of the helium star models for the *HST*/ACS filters of *F435W*, *F555W* and *F814W*, which roughly correspond to Johnson B, Johnson V, and Broad I filters, respectively (Sirianni et al. 2005). We computed the absolute magnitudes of the models in the VEGAMAG system using the synthetic model spectra and the transmission curves of the *HST*/ACS filters presented in Figure 1. For a filter P with a transmission curve of $P(\lambda)$, the absolute magnitudes in the VEGAMAG system are given by VEGAMAG(P) = $-2.5\log_{10}[\int P(\lambda)F_{\lambda}(\lambda)\lambda\, d\lambda / \int P(\lambda)F_{\lambda,\mathrm{Vega}}(\lambda)\lambda\, d\lambda]$, where F_{λ} and $F_{\lambda,\mathrm{Vega}}$ are the model flux from the CMFGEN calculations and the flux of Vega scaled to a distance of 10 pc (Sirianni et al. 2005). The reference spectrum of Vega is adopted from the SYNPHOT package distributed as a part of STSDAS[3]. We computed the bolometric magnitudes (M_{bol}) as well, assuming that the solar M_{bol} is 4.74 mag (Cox 2000), and present bolometric corrections in a given filter P ($\mathrm{BC}_P = M_{\mathrm{bol}} - \mathrm{VEGAMAG}(P)$) in Table 3.

For comparison, the magnitudes and bolometric corrections of the blackbody models are also presented in Table 3. The deviation from the blackbody model prediction depends on the strength of various lines, as well as the location of the actual photosphere for a given wind mass-loss rate. For example, if the photosphere were significantly lifted up with an optically thick wind that produces strong emission lines, the resulting luminosity in the optical would be much higher than in the corresponding case of blackbody. Otherwise, numerous absorption lines tend to decrease the visual brightness compared to what the blackbody models predict.

In general, for a given mass-loss rate, the optical thickness of a stellar wind becomes larger for a smaller radius of the star (e.g., Langer 1989). This explains why the difference between the stellar radius (R_*) and the photospheric radius (R_{phot}) becomes larger with a higher mass for a given

[3]http://www.stsci.edu/institute/software_hardware/stsdas/synphot

wind mass-loss rate as shown in Table 3. This also tends to make emission lines stronger. Therefore, the visual brightness of helium stars can be strongly influenced by winds, and the assumption of the blackbody may significantly underestimate the brightness of a helium star, as shown with M4w2 and M5w2 models. As also expected, for a given helium star mass, such difference becomes larger with a higher mass-loss rate: the w2 model tends to be brighter by up to ∼1 mag than the w1 model.

On the other hand, M3w1, M3w2 and M4w1 models have numerous absorption lines in their spectra, and their photosphere radii are not much different from the stellar radii (see Section 3 and Figures 2 and 3). Their visual brightness is comparable or a little fainter (∼0.3 mag) than the corresponding blackbody models, because of the presence of absorption lines and the lack of emission lines. The 3.0 $M_{\odot}$ model could be somewhat fainter than predicted in Table 3 if we included low-excitation species, which can produce more absorption lines in the spectra (see the above discussion on υ Sgr in Section 4). However, for more massive models, our result would not be affected with the inclusion of those species because the surface temperature is too high for the low-excitation lines to make any significant impact (e.g. Gray & Corbally 2009).

Note that the optical brightness becomes systematically lower for a higher helium star mass, and that the considered helium stars in the present study are predicted to be much brighter than massive single WR stars of WO type ($M_{\rm ZAMS} \gtrsim 30 - 35 M_{\odot}$) at the pre-SN stage that would have $M_{BVI} \simeq -3$ mag (Yoon et al. 2012; Groh et al. 2013b). The deepest absolute BVR magnitude limits of SN Ib/c progenitors in pre-explosion images to date are between −4 and −5 mag (Crockett et al. 2007; Eldridge et al. 2013), and they are comparable to the faintest one in our helium star models M5w1. Our work confirms the conclusion by Yoon et al. (2012) that the non-detection of SN Ib/c progenitors does not necessarily imply binary progenitors rather than massive WR progenitors. To the contrary, binary progenitors are easier to be found in the optical than massive WR progenitors of WO type that would be the most common type of SN Ib/c progenitors from single stars (Yoon et al. 2012; Eldridge et al. 2015). The probability of detecting binary SN Ib/c progenitors can further increase with a luminous O-type star companion as shown in Figure 5, while a significant fraction of binary progenitors would have a less luminous dwarf star or a compact object as a companion (Yoon 2015).

6. Comparison with the Progenitor Candidate of the Supernova iPTF13bvn

Cao et al. (2013) have recently reported a tentative identification of the progenitor of the SN Ib iPTF13bvn exploded in NGC 5806 (22.5 Mpc) from the pre-explosion *HST*/ACS images. The observed magnitudes of the object in *HST*/ACS *F435W*, *F555W*, and *F814W* images range from 26 to 27 mag depending on the adopted photometry method (Cao et al. 2013; Eldridge et al. 2015). The inferred absolute magnitudes range from -5.3 to -7.3 mag, given the uncertainties of the extinction towards NGC 5806. Cao et al. (2013) measured the Milky-Way (foreground) and the host galaxy reddening from the observed Na I D lines as $E(B-V)_{\rm MW} = 0.0278$ and $E(B-V)_{\rm host} = 0.0437$, whereas Bersten et al. (2014) adopted $E(B-V)_{\rm MW} = 0.0447$ (Schlafly & Finkbeiner 2011) and derived $E(B-V)_{\rm host} = 0.17 \pm 0.03$ using an intrinsic-color law from a sample of observed SNe. In this paper, we adopt the photometry results of Eldridge et al. (2015) and consider both values of reddening to compare the progenitor candidate of iPTF13bvn with our progenitor models. In Figure 5, we present the magnitude range of the iPTF13bvn progenitor candidate dereddened by the low ($E(B-V) = 0.0715$ from Cao et al. 2013) and high ($E(B-V) = 0.2147$ from Bersten et al. 2014) extinction values.

As shown in the figure, if we ignore the contribution from a companion star, only the 3.0 $M_{\odot}$ progenitor can marginally satisfy the observed magnitude range of the iPTF13bvn progenitor with the low-extinction. For the 4.4 $M_{\odot}$ and 5.1 $M_{\odot}$ progenitor, the companion star should be more massive than 20 $M_{\odot}$ and 30 $M_{\odot}$, respectively. With a 35 $M_{\odot}$ companion, all progenitor models give optical magnitudes compatible with those in the high-extinction case, but they are a bit too bright to fit with the low-extinction case. Therefore, for the considered mass range of helium stars, 35 $M_{\odot}$ roughly gives the upper limit of

the companion star mass. From the evolutionary point of view, a more massive helium star progenitor would systematically have a more massive companion if the binary system underwent stable mass transfers. For example, with stable Case B mass transfer systems [4], the upper limit of the companion star mass would be roughly about 27, 35 and 38 $M_\odot$, for 3.0, 4.4 and 5.1 $M_\odot$ helium star progenitors (see Yoon 2015, for more details on the binary progenitor evolution). With Case AB mass transfer systems[5], this limit would be higher by several solar masses (cf. Wellstein & Langer 1999). The lower limit of the companion star mass is zero: a helium star progenitor of the considered mass range would not have any companion if it were produced via Case A mass transfer that leads to reversal of the SN order as discussed by Pols (1994).

Considering both the theoretical constraint and the rather large magnitude uncertainty ($\sim$1 mag) resulting from the two extinction values, we conclude that a helium star progenitor of 3.0/4.4 $M_\odot$ with a 20/30 $M_\odot$ O-type star companion can best explain the observed magnitudes of the progenitor candidate in all the three *HST*/ACS filters. Their ($F435W-F555W$) and ($F555W-F814W$) colors presented in Figure 6 are also within the observed color ranges of the progenitor candidate, although all of the helium star binary progenitor models are distributed in a narrow color range.

Groh et al. (2013a) suggested a single WR star of WN type with initial masses of 31–35 $M_\odot$ as a progenitor of iPTF13bvn based on the predicted optical magnitudes ($M_{\rm V} \sim -5.5$ mag, gray dashed lines in Figure 5) of the non-rotating models from the Geneva stellar evolution code. We note that Groh et al. (2013a) used the photometry results from Cao et al. (2013), which are $\sim$1 mag fainter than those we present in this study based on Eldridge et al. (2015). While the predicted optical brightness is within the error bar of the observation, the final mass of this model ($\sim$11 $M_\odot$) is too high to explain the typical ejecta masses of SNe Ib/c ($M_{\rm ejecta}$ = 1–5 $M_\odot$; Drout et al. 2011; Cano 2013; Taddia et al. 2015) as well as the estimated ejecta mass of iPTF13bvn ($\sim$1.9–2.3 $M_\odot$; Bersten et al. 2014; Fremling et al. 2014).

Based on the SN ejecta mass and the optical brightness of the progenitor candidate, a binary progenitor with an initial mass of 10–20 $M_\odot$ for iPTF13bvn has been suggested (Bersten et al. 2014; Eldridge et al. 2015). Our stellar atmospheric modeling of low-mass helium stars ($M_{\rm final}$ = 3–4 $M_\odot$) with an O-type star companion of $\sim$ 20 – 30 $M_\odot$ also supports this scenario (Figures 5 and 6). Bersten et al. (2014) proposed the binary system composed of a 3.7 $M_\odot$ helium star ($T_{\rm eff} \sim 16,000$ K) and a 33.7 $M_\odot$ hot companion ($T_{\rm eff} \sim 44,000$ K) and predicted the SED of the progenitor at the pre-SN state. Their model (Figure 5 of Bersten et al. 2014) is fairly well consistent with the *HST*/ACS observations, but the assumption of a blackbody for the helium star may have uncertainty up to $\sim$1 mag as discussed in Secion 5. Figure 7 compares a predicted spectrum of one of our helium star binary models (M4w2+Ostar2) that reproduce best the observations of the iPTF13bvn progenitor candidate, which are dereddened by the low extinction value ($E(B-V) = 0.0715$). In the composite spectrum of the progenitor model, while the O-type star dominantly contributes the flux in the optical wavelengths, emission lines expected from the helium star appear in the spectrum; this makes the helium star binary system to be distinguishable from O-type stars with similar luminosity.

7. Conclusions

We have presented atmospheric models of relatively low-mass helium stars (3.0, 4.4, and 5.1 $M_\odot$) at the final evolutionary stage, which may represent typical SN Ib/c progenitors in binary systems. We confirm the prediction by Yoon et al. (2012) that these binary progenitors can be significantly brighter than more massive WR progenitors in the optical, and the visual brightness becomes higher for a less massive helium star progenitor because of the more extended envelope.

Their absolute magnitudes in the optical bands are comparable to those of 20 - 30 $M_\odot$ O-type stars ($M_V = -5 \sim -6$ mag). But unlike O-type stars, their spectra could be marked by strong emission lines if the mass-loss rate is sufficiently high. The envelopes of helium stars of 3 - 4 $M_\odot$ undergo rapid expansion during the late evolutionary

[4]Systems where mass transfer from the primary star starts during the helium core contraction phase.

[5]Systems where the first mass transfer starts during core hydrogen burning, followed by another mass transfer phase during helium core contraction.

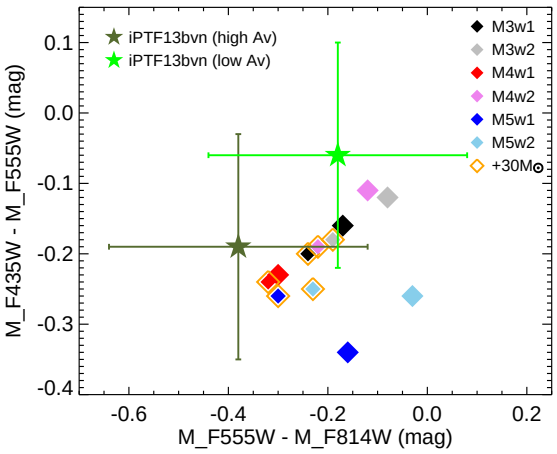

Fig. 6.— Color-color diagram of $(F435W - F555W)$ vs. $(F555W - F814W)$ of the helium star models without (filled diamonds) and with (filled diamonds with yellow borders) a 30 $M_\odot$ O-type star companion. Light and dark green filled stars are the colors of the iPTF13bvn progenitor candidate dereddened by the low and high extinction values (see the caption of Figure 5), respectively.

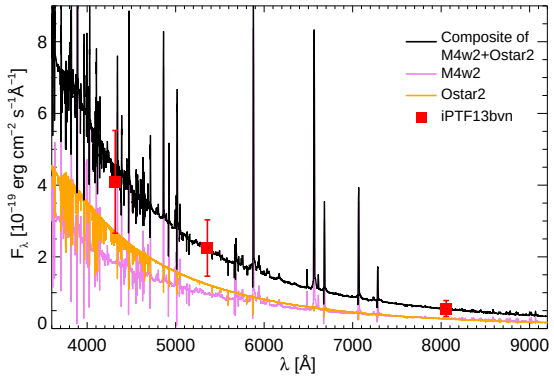

Fig. 7.— Predicted spectrum of the binary progenitor model composed of a 4.4 $M_\odot$ helium star and a 30 $M_\odot$ O-type star companion (M4w2+Ostar2 model). Pink and orange lines present the model spectra of the helium star and O-type star, respectively, and the black line is the composite spectrum of the two. The *HST*/ACS observations of the iPTF13bvn progenitor candidate (Eldridge et al. 2015) dereddened by low-extinction value of $E(B-V) = 0.0715$ (Cao et al. 2013) are compared with red squares.

stages to become a helium giant ($R \simeq 10 - 50\ R_\odot$; Yoon et al. 2010, 2012; Eldridge et al. 2015), and the resulting emission lines would be fairly narrow, compared to those of typical WR stars (Figures 2 and 3).

We compared our results with the observational properties of the progenitor candidate of the SN Ib iPTF13bvn. We find that models with 3.0/4.4 $M_\odot$ helium star plus a 20/30 $M_\odot$ O-type star companion give the best fit with the observation in terms of magnitudes and colors, in good agreement with Bersten et al. (2014), but a 3.0 $M_\odot$ helium star progenitor can also have optical magnitudes comparable to those of the iPTF13bvn progenitor even without an O-type star companion (see also Eldridge et al. 2015, for a similar conclusion), depending on the degree of extinction to the source.

Future observations might find the surviving O-type star companion of the iPTF13bvn progenitor. According to our prediction, its optical brightness should be lower by about $\Delta M = 0.2 - 0.9$ mag than that of the observed brightness of the iPTF13bvn progenitor, depending on the combination of the helium star and O-type star masses. This is because the contribution from the helium star progenitor must have disappeared. If no meaningful change in the optical magnitudes of the source is found in the future, it may indicate either that the iPTF13bvn progenitor was more massive than about 5 $M_\odot$ while the source was the O-type companion star of $\sim$ 35 $M_\odot$, or that the source was not associated with iPTF13bvn at all. A caveat in this argument is that the luminosity of the companion star might have been significantly influenced by the interaction with the SN ejecta, and that there even exists the possibility that the source appears somewhat more luminous than in the pre-SN image, because of the shock heating in the companion star (Hirai & Yamada 2015).

However, as discussed above, a $\sim 3\ M_\odot$ helium star alone without a luminous companion can also explain the optical brightness of the iPTF13bvn progenitor in principle and non-detection of the surviving companion star would not necessarily imply a single star progenitor because the companion could be a faint dwarf star or a compact object (Eldridge et al. 2013; Yoon 2015). With reversal of the SN order in a Case A binary system, such a relatively low-mass helium star progenitor

produced in a binary system might not even have any companion at the pre-SN stage (Pols 1994).

One important question still remains to be answered: if binary progenitors can be so bright in the optical as predicted by our models and if they represent typical SN Ib/c progenitors, why have they been so elusive in the previous searches? The detection limits were $M_{\rm B} \simeq -4.4$ mag and $M_{\rm R} \simeq -4.92$ mag in the searches of the progenitors of SN 2002ap and SN 2010br, respectively (Eldridge et al. 2013). They would have been detected, if their masses were about 3 $M_{\odot}$ (see Figure 5), even without a luminous companion. However, all of the other searches had more severe detection limits ($M_{\rm BVRI} \lesssim -6.5$ mag), and the progenitors would have been detected only with an O-type star companion of $M \gtrsim 20 - 30\ M_{\odot}$. The previous difficulty in detecting a SN Ib/c progenitor might have resulted from the fact that most SN Ib/c progenitors in binary systems do not have a luminous O-type star companion. It should also be noted that SN Ic progenitors would be generally more difficult to detect than SN Ib progenitors. This is because SN Ib progenitors would have a fairly massive helium envelope that results in large radii at the pre-SN stage (hence high optical luminosities), while SN Ic progenitors that are helium-deficient would remain very hot and faint in the optical (Yoon et al. 2012). SN 2002ap was a SN Ic, and therefore it is not surprising that its progenitor could not be detected even with such a deep search. This issue should be addressed more carefully with a binary population synthesis model that fully takes into account the evolutionary effects on the helium star structure at the final evolutionary stage and the recent observational constraints on the SN Ib/c ejecta masses (cf. Kochaneck 2009; Yoon et al. 2012; Eldridge et al. 2013).

The authors are grateful to John Hillier for making the CMFGEN code publicly available, to John Eldridge and Melina Bersten for communicating their results and to the anonymous referee for many useful comments that helped us improve the paper. S.-C. Y was supported by the Basic Science Research (2013R1A1A2061842) program through the National Research Foundation of Korea (NRF). B.-C. K was supported by Basic Science Research Program through the National Research Foundation of Korea(NRF) funded by the Ministry of Science, ICT and future Planning (2014R1A2A2A01002811). H.-J. K was supported by NRF(National Research Foundation of Korea) Grant funded by the Korean Government (NRF-2012-Fostering Core Leaders of the Future Basic Science Program). This work has made use of the BeSS database, operated at LESIA, Observatoire de Meudon, France: http://basebe.obspm.fr.

REFERENCES

Bersten, M. C., Benvenuto, O. G., Folatelli, G., et al. 2014, AJ, 148, 68

Bonneau, D., Chesneau, O., & Mourard, D. et al. 2011, A&A, 532, A148

Branch et al. 2002, ApJ, 566, 1005

Cano, Z. 2013, MNRAS, 434, 1098

Cao, Y., Kasliwal, M. M., Arcavi, I., et al. 2013, ApJ, 775, LL7

Cox, A. N. 2000, Allen's Astrophysical Quantities (4th ed.; New York:Springer)

Crockett, R. M., Smartt, S. J., Eldridge, J. J., et al. 2007, MNRAS, 381, 835

Deng,J.S., Qui, Y.L., Hu, J.Y., Hatano, K., & Branch, D. 2000, ApJ, 540, 452

Dessart, L., Hillier, D.J., Livne, E., Yoon, S.-C., Woosley, S.E., Waldman, R., & Langer, N. 2011, MNRAS, 414, 2985

Drout, M. R., Soderberg, A. M., Gal-Yam, A., et al. 2011, ApJ, 741, 97

Dudley, R. E., & Jeffery, C. S. 1993, MNRAS, 262, 945

Eldridge, J.J., Izzard, R.G., & Tout, C.A. 2008, MNRAS, 383, 1109

Eldridge, J. J., Fraser, M., Maund, J. R., & Smartt, S. J. 2015, MNRAS, 446, 2689

Eldridge, J. J., Fraser, M., Smartt, S. J., Maund, J. R., & Crockett, R. M. 2013, MNRAS, 436, 774

Elmhamdi, A., Danziger, I.J., Branch, D., Leibundgut, B., Baron, E., & Kirchner, R.P. 2006, A&A, 450, 305

Foley, R.J., Smith, N., Ganaeshalingam, M., Li., W., Chornock, R., & Filippenko, A.V. 2007, ApJ, 657, 105

Fremling, C., Sollerman, J., Taddia, F., et al. 2014, A&A, 565, AA114

Gorbikov, E. et al. 2014, MNRAS, 443, 671

Gray, R.O., & Corbally, C.J. 2009, Stellar Spectral Classification, Princeton Series in Astrophysics

Groh, J. H., Georgy, C., & Ekström, S. 2013a, A&A, 558, LL1

Groh, J. H., Meynet, G., Georgy, C., & Ekström, S. 2013b, A&A, 558, AA131

Groh, J. H., Oliveira, A. S., & Steiner, J. E. 2008, A&A, 485, 245

Hamann, W.-R., Koesterke, L., & Wessolowski, U. 1995, A&A, 116, 273

Hamann, W.-R., Gräfener, G., & Liermann, A. 2006, A&A, 457, 1015

Hillebrandt, W., & Niemeyer, J.C. 2000, ARA&A, 38, 191

Hillier, D. J., & Miller, D. L. 1998, ApJ, 496, 407

Hillier, D. J. 1990, A&A, 231, 116

Hillier, D. J. 2003, in ASP Conf. Ser. 288, Stellar Atmosphere Modeling, eds. I. Hubeny, D. Mihalas, & K. Werner, 199

Hirai, R., & Yamada, S. 2015, ApJ, in press, arXive:1504.01845

Kipper, T., & Klochkova, V. G. 2012, Baltic Astronomy, 21, 219

Kobulnicky, H.A., & Fryer, C.L. 2007, ApJ, 670, 747

Kochanek, C. 2009, ApJ, 707, 1578

Langer, N. 1989, 210, 93

Lyman, J., Bersier, D., & James, P. et al. 2014, arXive:1406.3667

Pols, O.R. 1994, A&A, 290, 119

Pastorello, A., Mattila, S., & Zampieri, L. et al. 2008, MNRAS, 389, 113

Podsiadlowski, Ph., Joss, P.C., & Hsu, J.J.L. 1992, ApJ, 391, 246

Saio, H. 1995, MNRAS, 277, 1393

Sana et al. 2012, Science, 337, 444

Sander, A., Hamann, W.-R., & Todt, H. 2012, A&A, 540, AA144

Schlafly, E. F., & Finkbeiner, D. P. 2011, ApJ, 737, 103

Sirianni, M., Jee, M. J., Benítez, N., et al. 2005, PASP, 117, 1049

Smartt, S. J. 2009, ARA&A, 47, 63

Smith, N., Li, W., Filippenko, A.V., & Chornock, R. 2011, MNRAS, 412, 1522

Spencer, J. & Baron, E. 2010, ApJ, 718, 957

Steiner, J. E., & Oliveira, A. S. 2005, A&A, 444, 895

Taddia, F., Sollerman, J., & Leloudas, G et al. 2015, A&A, 574, A60

Vink, J.S., & de Koter, A. 2005, A&A, 442, 587

Wellons, S., Soderberg, A.M. & Chevalier, R.A. 2012, ApJ, 752, 17

Wellstein, S. & Langer, N. 1999, A&A, 350, 148

Willis, A. J., & Stickland, D. J. 1983, MNRAS, 203, 619

Woosley, S.E., Langer, N., & Weaver, T.A. 1995, ApJ, 448, 315

Yoon, S.-C., 2015, PASA, 32, 15

Yoon, S.-C., Gräfener, G., Vink, J. S., Kozyreva, A., & Izzard, R. G. 2012, A&A, 544, L11

Yoon, S.-C., Woosley, S. E., & Langer, N. 2010, ApJ, 725, 940

This 2-column preprint was prepared with the AAS LaTeX macros v5.2.

Table 1
Model Parameters

Model	$M_\star$ ($M_\odot$)	$L_\star$ ($L_\odot$)	$T_\star$[a] (K)	$T_{\rm eff}$[b] (K)	$R_\star$[a] ($R_\odot$)	$R_{\rm phot}$[b] ($R_\odot$)	$\dot{M}$ ($M_\odot$ yr^{-1})	v_∞ (km s^{-1})	β[c]	$X_{\rm H}$[d]	$X_{\rm He}$[e]	$X_{\rm C}$[f]	$X_{\rm N}$[g]	$X_{\rm O}$[h]
M3w1	3.0	4.45e+04	15057	15060	30.97	30.97	6.57e-07	386.51	1.0	7.26e-02	9.09e-01	1.55e-04	1.33e-02	3.71e-04
M3w2	3.0	4.45e+04	15057	14990	30.97	31.22	1.00e-05	289.88	1.5	7.26e-02	9.09e-01	1.55e-04	1.33e-02	3.71e-04
M4w1	4.4	9.05e+04	28596	28590	12.26	12.25	1.50e-06	452.57	1.0	1.10e-01	8.72e-01	1.22e-04	1.33e-02	4.00e-04
M4w2	4.4	9.05e+04	28596	22630	12.26	19.55	2.00e-05	339.43	1.5	1.10e-01	8.72e-01	1.22e-04	1.33e-02	4.00e-04
M5w1	5.1	1.12e+05	50587	49520	4.35	4.54	4.88e-06	1332.76	1.0	7.35e-06	9.81e-01	2.46e-04	1.32e-02	2.94e-04
M5w2	5.1	1.12e+05	50587	39430	4.35	7.16	2.00e-05	999.57	1.5	7.35e-06	9.81e-01	2.46e-04	1.32e-02	2.94e-04
Ostar1	20.0	7.05e+04	29402	29400	10.23	10.22	1.50e-07	1714.39	1.0	7.01e-01	2.80e-01	3.48e-03	1.03e-03	1.00e-02
Ostar2	30.0	1.99e+05	32088	32090	15.00	14.41	6.00e-07	1718.73	1.0	7.01e-01	2.80e-01	3.48e-03	1.03e-03	1.00e-02
Ostar3	35.0	3.72e+05	28610	28610	24.84	24.82	1.13e-06	1458.47	1.0	6.46e-01	3.36e-01	1.99e-03	3.99e-03	8.29e-03

Note.—All the parameters except $T_{\rm eff}$ and R_* are taken from the stellar evolueionary models of Yoon et al. (2010) and used as the input parameters for the CMFGEN calculations. $T_{\rm eff}$ and $R_{\rm phot}$ are the outputs from the calculations.

[a] From the stellar evolution code (Yoon et al. 2010) without correcting the optical depth effects from the wind.

[b] Effective temperature and photospheric radius from the CMFGEN calculations defined at the Rosseland optical depth = 2/3.

[c] From the standard β-type velocity law. β=1 and 1.5 for w1 and w2 models, respectively.

[d,e,f,g,h] Mass fraction of hydrogen, helium, carbon, nitrogen, and oxygen.

Table 2
Model Atoms Used in CMFGEN Calculation

Species	Super Levels	Full Levels
H I	20	30
He I	45	69
He II	22	30
C II	40	92
C III	51	84
C IV	59	64
N II	45	85
N III	41	82
N IV	44	76
N V	41	49
O II	54	123
O III	88	170
O IV	38	78
O V	32	56
O VI	25	31
Si III	33	33
Si IV	22	33
Fe III	104	1433
Fe IV	74	540
Fe V	50	220
Fe VI	44	433
Fe VII	29	153

Note.—The second column denotes the total number of super levels, which mean the energy levels that was used for the calculation. In the calculation, some levels having similar excitation energies are grouped into a single super level, to save computing time. In the case of H I, for example, 30 levels are considered in the calculation. For the first 15 levels, each super level corresponds to the actual energy level of H I, but the super levels from 16 to 20 correspond to the grouped levels for 16–18, 19–21, 22-24, 25–27, and 28–30, respectively. Therefore, the total number of super levels used for the computation is 20, while the total number of the considered energy levels is 30, which is given in the third column.

TABLE 3

ABSOLUTE MAGNITUDES AND BOLOMETRIC CORRECTIONS OF THE MODELS AND THE BLACKBODY APPROXIMATIONS IN THE *HST*/ACS *F435W*, *F555W*, AND *F814W* FILTERS.

Model	M_{F435W} (mag)	M_{F555W} (mag)	M_{F814W} (mag)	BC_{F435W} (mag)	BC_{F555W} (mag)	BC_{F814W} (mag)
M3w1	-5.87	-5.71	-5.54	-1.01	-1.17	-1.34
M3w2	-5.85	-5.73	-5.65	-1.03	-1.15	-1.23
M4w1	-5.21	-4.98	-4.68	-2.44	-2.67	-2.97
M4w2	-5.53	-5.42	-5.30	-2.12	-2.23	-2.35
M5w1	-4.13	-3.79	-3.63	-3.75	-4.09	-4.25
M5w2	-4.83	-4.57	-4.54	-3.05	-3.31	-3.34
Ostar1	-4.86	-4.61	-4.28	-2.52	-2.77	-3.10
Ostar2	-5.79	-5.54	-5.22	-2.72	-2.97	-3.29
Ostar3	-6.75	-6.52	-6.22	-2.44	-2.67	-2.97
In binary systems (from composite spectra)						
M3w1+Ostar1	-6.23	-6.05	-5.83	···	···	···
M3w2+Ostar1	-6.22	-6.06	-5.92	···	···	···
M4w1+Ostar1	-5.80	-5.56	-5.25	···	···	···
M4w2+Ostar1	-6.00	-5.84	-5.66	···	···	···
M5w1+Ostar1	-5.31	-5.03	-4.75	···	···	···
M5w2+Ostar1	-5.60	-5.34	-5.17	···	···	···
M3w1+Ostar2	-6.58	-6.38	-6.14	···	···	···
M3w2+Ostar2	-6.57	-6.39	-6.20	···	···	···
M4w1+Ostar2	-6.29	-6.05	-5.73	···	···	···
M4w2+Ostar2	-6.42	-6.23	-6.01	···	···	···
M5w1+Ostar2	-6.00	-5.74	-5.44	···	···	···
M5w2+Ostar2	-6.16	-5.91	-5.68	···	···	···
M3w1+Ostar3	-7.15	-6.94	-6.68	···	···	···
M3w2+Ostar3	-7.14	-6.95	-6.72	···	···	···
M4w1+Ostar3	-6.98	-6.76	-6.45	···	···	···
M4w2+Ostar3	-7.05	-6.86	-6.60	···	···	···
M5w1+Ostar3	-6.84	-6.60	-6.31	···	···	···
M5w2+Ostar3	-6.92	-6.69	-6.43	···	···	···
Blackbody[a]						
BB_M3	-5.91	-5.85	-5.81	-0.97	-1.03	-1.07
BB_M4	-5.32	-5.10	-4.85	-2.33	-2.55	-2.80
BB_M5	-4.01	-3.72	-3.38	-3.87	-4.16	-4.50

[a]Based on the blackbody fluxes for the given temperature ($T_\star$) and luminosity of 3.0, 4.4, and 5.1 $M_\odot$ models in Table 1.